mater.scichina.com link.springer.com

Published online 18 January 2023 | https://doi.org/10.1007/s40843-022-2328-8
Sci China Mater 2023, 66(5): 1923–1933

Highly sensitive and self-healing conductive hydrogels fabricated from cationic cellulose nanofiber-dispersed liquid metal for strain sensors

Shihao Wu[1†], Bingyan Wang[1†], Duo Chen[2], Xiaona Liu[1], Huili Wang[1], Zhaoping Song[1], Dehai Yu[1], Guodong Li[1], Shaohua Ge[3] and Wenxia Liu[1*]

ABSTRACT The emergence of liquid metal (LM) emulsion as a soft multifunctional filler brings a new opportunity for fabricating hydrogel-based strain sensors with multifunctional properties. However, the extremely large surface tension and high density of LMs inhibit emulsification. Herein, we demonstrated a strategy for stabilizing LM emulsions using cationic cellulose nanofibers (CCNFs) to encapsulate LM droplets through strong electrostatic attraction with LM. By inducing acrylic acid (AA) polymerization in the presence of a CCNF-stabilized LM emulsion, a conductive hydrogel was prepared with the formation of reversible hydrogen bonds, ionic coordination, and electrostatic interactions among CCNFs, LM droplets, and poly(acrylic acid) (PAA). The hydrogel obtained, named the CCNF-LM-PAA hydrogel, shows good conductivity (1.54 S m^{-1}), remarkable tensile strength and elongation at break, self-adhesiveness, and quick self-healing capability. As a strain-sensing material, the CCNF-LM-PAA hydrogel exhibits a very high sensing sensitivity (gauge factor = 16.2), a low strain detection limit (less than 1%), a short response/recovery time (107/91 ms), and good durability (300 cycles). These results enable the CCNF-LM-PAA hydrogel-based strain sensor to be an excellent wearable device for monitoring various human activities. Therefore, introducing additional electrostatic interactions by using CCNFs to stabilize LM emulsions provides a practical way to enhance the strain-sensing performance of LM emulsion-based hydrogels for assembling self-attached wearable devices.

Keywords: hydrogel, liquid metal, emulsion, cationic cellulose nanofibers, strain sensor, self-healing

INTRODUCTION

In recent decades, artificial intelligence technology [1], soft robotics [2,3], wearable devices [4,5], and implantable biomedical devices [6] have undergone rapid development, making skin-like materials an important medium for human-machine interactions [7] and receiving extensive attention from industry and academia. When acting as the substrates/matrices of electronic skins, which are multiple strain sensors that can mimic the sensory characteristics of human skin and convert external stimuli such as pressure [8], strain [9,10], vibration [11], temperature [12,13], and humidity [14,15] into detectable electrical signals, skin-like materials are generally required to show low toxicity/good biocompatibility, good mechanical properties, and long-term stability. Meanwhile, to avoid accidental damage to electronic skin during use, skin-like materials must be imparted with self-healing properties, which in turn substantially improve the durability and service life of electronic skin [16–19].

Polymeric hydrogel is an ideal skin-like material as the matrix of a flexible strain sensor because of its good biocompatibility, softness, and strong similarity to wet tissue [20–22]. The polymeric hydrogel possesses a three-dimensional (3D) polymer network, which has the remarkable characteristics of viscoelasticity and hydrophilicity [23–25]. Hydrogels with polymer chains crosslinked through noncovalent bonding and dynamic covalent bonding can easily be self-healed by regaining their structure after they are damaged [26,27]. Meanwhile, by incorporating conductive materials into the polymeric network, conductive hydrogels can be prepared for direct use as the sensing material of a strain sensor [28,29]. Conductive materials, such as carbon-based materials, MXenes, metal nanoparticles/nanowires, and liquid metals (LMs), and conductive polymer-based materials have been introduced into the insulating hydrogel matrix as conductive fillers for strain sensor fabrication [30–32]. In addition to providing conductivity for hydrogels, conductive materials also substantially affect the mechanical and self-healing properties of hydrogels. Among the reported conductive materials, LMs such as gallium and its eutectic alloys have attracted increasing attention in fabricating strain sensors as soft fillers of conductive hydrogels because of their high conductivity, negligible toxicity, excellent antibacterial properties, and good matching with the polymer matrix of stretchable hydrogels [33–36]. In addition, LMs and their derivatives show strong interactions with chemical groups such as $-NH_2$, –OH, and –COOH, which are conducive to forming strong conductive hydrogels by producing good interfacial interactions between LM and the polymer matrix [37–40]. Meanwhile, LMs can produce active radicals and Ga^{3+} under sonication, which allows

[1] State Key Laboratory of Biobased Materials and Green Papermaking, Qilu University of Technology, Shandong Academy of Sciences, Jinan 250353, China
[2] Department of Optoelectronic Science and Technology, Qilu University of Technology, Shandong Academy of Sciences, Jinan 250353, China
[3] Department of Periodontology, School and Hospital of Stomatology, Cheeloo College of Medicine, Shandong University & Shandong Key Laboratory of Oral Tissue Regeneration & Shandong Engineering Laboratory for Dental Materials and Oral Tissue Regeneration, Jinan 250012, China
† These authors contributed equally to this work.
* Corresponding author (email: liuwenxia@qlu.edu.cn)

an extremely rapid *in situ* formation of conductive hydrogels at room temperature by promoting the monomer polymerization and offering hydrogels with self-healing properties by ionically crosslinking the formed polymers [8,33,41]. However, LMs are featured as a water-insoluble fluid with low viscosity, high density, and extremely large surface tension. To be uniformly integrated into hydrogels as a droplet filler, the continuous LMs must be dispersed in the aqueous phase under the protection of surface-active substances through high shear or sonication to form stable LM emulsions [41].

Because of the interaction of LMs with $-NH_2$, –OH, and –COOH, polar monomers such as acrylic acid (AA) [41] and acrylamide (AM) [42] have been used to keep the LM droplets stable when polymerized *in situ*, and crosslinked polyacrylamide (PAM) and poly(acrylic acid) (PAA) have been employed as the polymeric matrix of hydrogels. Unfortunately, polar monomers only provide a limited stabilization effect on LM emulsions because of the extremely large surface tension and high density of LMs, which inevitably induce gravitational sedimentation and the coalescence of LM droplets [8,42]. Consequently, the LM-based hydrogels obtained show limited sensitivity (gauge factor, GF). Using hydrophilic polymers such as polyvinyl alcohol (PVA) [38], tannic acid-crosslinked PVA [39], and epichlorohydrin-crosslinked chitosan quaternary ammonium salt [43] to stabilize LM droplets or using carboxymethylcellulose (CMC) [44] to costabilize LM droplets with AM can substantially reduce the sedimentation and coalescence of LM droplets. However, the stretchability of the conductive hydrogels obtained is rather low, probably because of the low flexibility of crosslinked PVA and chitosan quaternary ammonium salt, where they solely constitute the polymeric matrices of the corresponding conductive hydrogels, or because of double network formation with reduced stretchability by stiff CMC and *in situ* synthesized and crosslinked PAM. Meanwhile, hydrophilic particles such as dialdehyde xylan [45], graphene oxide [46,47], and (2,2,6,6-tetramethylpiperidin-1-yl)oxidanyl-oxidized cellulose nanofibers (CNFs) [48] have also been employed to stabilize LM droplets, while poly(3,4-ethylenedioxythiophene):sulfonated bacterial CNF (PEDOT:BCNF) has been used to costabilize LM droplets with AA [34]. Interestingly, these hydrophilic particles provide good protection effects for the LM droplets by forming mechanical barriers, preventing the LM droplets from undergoing sedimentation and coalescence [33,45]. However, these hydrophilic particles generally carry negative charges, which impair their interactions with LM droplets by reducing electrostatic attraction.

To fully use LM as a multifunctional filler, herein, we develop a new strategy for stabilizing LM emulsions by encapsulating LM droplets with cationic CNFs (CCNFs) rich in quaternary ammonium groups, which induce strong ion-dipole/electrostatic interactions with LM droplets and provide mechanical barriers to prevent the LM droplets from coalescing and undergoing sedimentation. During the LM emulsifying process, ultrasonic treatment is applied to break bulk LM into droplets and produce active radicals and gallium oxide. The active radicals enable vinyl monomer—AA to polymerize at room temperature, while the gallium oxide reacts with the AA to form Ga^{3+}, which not only provides ionic conductivity for hydrogels but also induces quick gelatinization by ionic crosslinking among PAA molecules, intriguing the development of self-healing and adhesive behaviors for the as-prepared hydrogels. Meanwhile, CCNFs simultaneously act as a reinforcing agent to constitute a double network structure with *in situ* synthesized PAA for fabricating LM droplet-based conductive hydrogels by additionally introducing reversible electrostatic interactions with PAA. Because of the high aspect ratio and strong interaction with LM droplets and PAA, the CCNFs not only prevent the sedimentation and coalescence of LM droplets but also improve the interfacial compatibility between the LM droplets and the PAA matrix, enabling the as-prepared CCNF-LM-PAA hydrogels to possess ultrahigh sensing performance in addition to showing high stretchability, good self-healing ability, and self-adhesiveness. Therefore, using CCNFs to encapsulate LM droplets opens a new window to quickly and easily fabricating multifunctional conductive hydrogels for highly sensitive strain sensors.

EXPERIMENTAL SECTION

Materials

CCNFs with a diameter of 10–20 nm and a length of 10–20 μm were procured from Tianjin Woodelf Biotechnology Co., Ltd. (Tianjin, China) as an aqueous dispersion at a concentration of 1.35 wt%. According to the supplier, the CCNFs were made from softwood pulp and had a cationic charge density of 0.480 mmol g^{-1}. LM (99.99% Ga) was purchased from Guangzhou Lige Technology Co., Ltd. (Guangzhou, China). AA (>99%) was purchased from Guangzhou Sopo Biolog Technology Co., Ltd. (Guangzhou, China). Ammonium persulfate (APS, >98%) was obtained from Shanghai Macklin Biochemical Co., Ltd. (Shanghai, China). All the reagents were used as received.

Preparation of CCNF-stabilized LM emulsions

A CCNF-stabilized LM emulsion was prepared by sonication [8]. Typically, 0.2 g of Ga was added to 7 mL of a CCNF aqueous dispersion. The mixture was then sonicated for 15 min using a cell fragmentation instrument (JY92-IIN, Shanghai, China) with a power of 500 W in an ice-water bath. By changing the concentration of the CCNF aqueous dispersion or the amount of the added Ga, Ga emulsions with different CCNF concentrations and amounts of added Ga were prepared.

Preparation of CCNF-LM-PAA hydrogels

CCNF-LM-PAA hydrogels were fabricated by AA polymerization, hydrogen bonding, ionic crosslinking, and electrostatic interaction-induced gelatinization. In a typical process, 2.7 mL of AA was added to 7 mL of CCNF-stabilized Ga emulsion, followed by the addition of 0.025 g of APS under stirring. After blending for a few seconds, the mixture was poured into a mold and stood at room temperature for gelatinization, which occurred quickly.

Characterization

The morphologies and structures of the as-prepared CCNF-stabilized LM emulsion and CCNF-LM-PAA hydrogel were analyzed using scanning electron microscopy (SEM) and microcomputed tomography (micro-CT). The SEM images were recorded on a Hitachi Regulus 8220 scanning electron microscope (Hitachi, Tokyo, Japan). 3D images of the CCNF-LM-PAA hydrogels were collected using a microCT system (Sky-Scan2211, Bruker, Munich, Germany). The stress-strain curves of various hydrogel samples with a length of 15 mm and width of 4 mm were plotted using the data collected from tensile tests

performed using a Texture Analyzer (TA. XT Plus C, Stable Micro Systems, Surrey, UK) operated at a speed of 20 mm min^{-1}.

Sensing performance measurements

The sensing performance of the CCNF-LM-PAA hydrogels acting as sensing materials was evaluated through their real-time response to applied strain. The real-time resistance of CCNF-LM-PAA hydrogel samples with dimensions of 15 mm × 5 mm × 5 mm was recorded using a designed system composed of a texture analyzer (TA. XT Plus C, Stable Micro Systems, the United Kingdom), a computer, and a digital source meter (2450, Keithley Co., Solon, OH, USA).

RESULTS AND DISCUSSION

Preparation and characterization

CCNF-LM-PAA hydrogels were produced by dispersing Ga in a CCNF aqueous dispersion under sonication, followed by mixing with AA and APS to induce *in situ* AA polymerization by APS in the presence of Ga droplets at room temperature, as shown in Fig. 1a, where *in situ* polymerized and crosslinked PAA and CCNFs act as the soft and hard polymeric networks of the hydrogel, respectively. In this system, the CCNF-LM-PAA-hydrogel is constructed by CCNF-stabilized LM droplet-reinforced PAA-CCNF double networks, which form through ionic coordination, hydrogen bonds, and electrostatic/ion-dipole interactions, as shown in Fig. 1b.

As an active metal, Ga is easily oxidized to form a thin oxide layer in the presence of oxygen [49]. When Ga was dispersed into a CCNF aqueous dispersion under sonication, Ga_2O_3 was formed on the LM droplet surfaces, as confirmed by the X-ray photoelectron spectroscopy spectra shown in Fig. S1-i–iii. The presence of Ga_2O_3 on LM droplet surfaces makes the LM droplets produce hydrogen bonding and ion-dipole/electrostatic interactions with CCNFs in the emulsification process of LM, allowing the formation of a stable LM emulsion under sonication. CCNF-stabilized LM emulsion formation enables LM to uniformly mix with AA as a conductive filler and as a binding site to connect CCNFs and PAA, while the LM droplets simultaneously promote AA monomer polymerization in the presence of persulfate radical initiators, probably due to the redox catalysis of Ga for persulfate to generate radicals, enabling PAA to form at room temperature [8,47]. Furthermore, the LM droplets can react with H^+ generated by –COOH ionization of AA to generate Ga^{3+}, which can be confirmed by the substantially increased Ga(III) in the gelatinization process of CCNF-LM-PAA, as shown in Fig. S1-iv–vi. Ga^{3+} can coordinate with $–COO^-$ to ionically crosslink PAA, while the quaternary ammonium groups of CCNFs can electrostatically interact with $–COO^-$, resulting in the formation of CCNF- and PAA-based supramolecular double networks [50]. Consequently, the CCNF-LM-PAA hydrogel is rapidly formed at room temperature (Fig. S2).

Fig. 2a shows the appearance of CCNF-stabilized LM emulsions with the CCNF concentration of 0.2 wt% and 0.2 g of Ga (the CCNF:Ga mass ratio is 0.14:2) under different standing times. As shown in Fig. 2a, the CCNF-stabilized Ga droplets remain well dispersed for at least 48 h, while the Ga droplets without CCNF protection precipitate quickly, confirming the excellent stabilization effect of CCNFs on Ga droplets due to the strong interaction of Ga and Ga_2O_3 with the hydroxyl groups [8,41] and the quaternary ammonium groups of CCNFs [43].

Fig. 2b shows the SEM images of the same CCNF-stabilized LM emulsion. Apparently, the Ga droplets have a diameter of 0.25–1.0 μm and possess a regular spherical shape with CCNFs covering their surfaces. CCNFs form mechanical barriers to prevent the Ga droplets from coalescing and undergoing sedimentation [33]. Meanwhile, CCNFs are also present in the continuous phase, allowing them to be a part of the CCNF-LM-PAA hydrogel matrix. The Ga droplets, together with their CCNF coverage, not only accelerate the formation of the hydrogel as the source of free radicals but also participate in the formation of the hydrogel as an important component. Therefore, the LM droplets inhabit mainly the polymeric matrix of the hydrogel, as shown in the SEM image of the cross-sectional CCNF-LM-PAA hydrogel with a CCNF:Ga:AA mass ratio of 0.14:2:27 after being freeze-dried (Fig. 2c). The Ga distribution in the hydrogel was further characterized using energy dispersive X-ray spectroscopy (EDS) elemental mapping (Fig. 2d, e). As shown in Fig. 2d, e, the Ga atoms are evenly dispersed in the polymeric matrix composed of C and O atoms. Fig. 2f shows the micro-CT image of the hydrogel, which further illustrates the uniform dispersion of Ga in the hydrogel.

Fig. 2g shows that the CCNF-LM-PAA hydrogel can be molded into various shapes, indicating the good moldability of the hydrogel originating from controllable gelatinization. Adhesiveness is a crucial property for new wearable sensors directly adhering to skin without using adhesive tape or bandages in monitoring large-range human motion [50,51]. The CCNF-LM-PAA hydrogel, as shown in Fig. 2h and Fig. S3a, has good adhesiveness to various surfaces, such as skin, metal, wood, glass, paper, plastic, and rubber, and can easily stick to human skin and bear a weight of 200 g without falling off. The good adhesiveness of the CCNF-LM-PAA hydrogel to various substrates is attributed to its combined performance in forming chemical bonds and a mechanical interlock with joint surfaces, as well as energy dissipation in deformation [46]. The CCNF-LM-PAA hydrogel can form hydrogen bonds, ionic coordination, and ion-dipole/electrostatic interactions with various substrate interfaces because of the presence of Ga^{3+} and numerous functional groups, such as carboxyl, hydroxyl, and quaternary ammonium groups, in the hydrogel [52,53]. The formation of a mechanical interlock with rough surfaces originates from the good moldability of the CCNF-LM-PAA hydrogel, which can fill the pits before gelatinization. The double network structure and the strong interactions among CCNF, LM, and PAA contribute a high-energy dissipation in the separation of bonded CCNF and PAA and the slipping and detaching of the CCNFs and PAA from the surface of LM droplets [46]. Quantitative measurements of the adhesiveness further reveal that the adhesive strength of the CCNF-LM-PAA hydrogel to plastic, wood, paper, glass, and rubber is 0.05, 14, 1.92, 0.554, and 0.101 MPa, respectively (Fig. S3b). CCNF-LM-PAA hydrogel has a higher adhesive strength to wood, paper, and glass than to plastic and rubber because of the larger amount of hydrophilic functional groups of the former substances, particularly hydroxyl groups, which form more chemical bonds with the hydrogels. The hydrogel has a higher adhesive strength to wood than to paper because of the rougher surfaces of the former substance. Meanwhile, the CCNF-LM-PAA hydrogel is highly stretchable. As shown in Fig. 2i, the 2-cm-wide hydrogel is stretched to

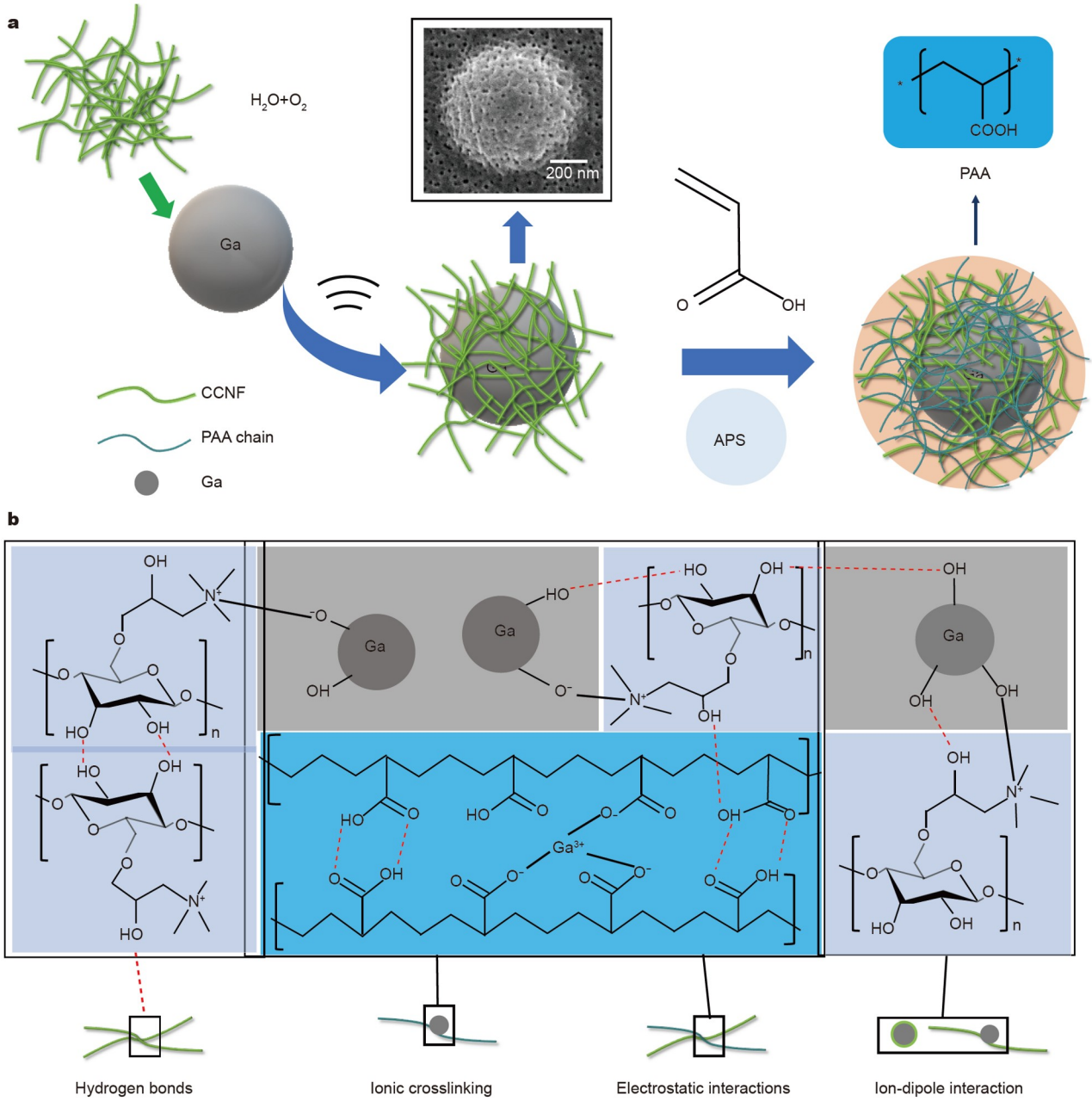

Figure 1 Schematics of (a) CCNF-LM-PAA hydrogel preparation and (b) the interactions among CCNFs, LM droplets, and PAA.

30 cm, proving its excellent stretching capacity. During the stretching process, the hydrogel becomes longer and thinner, leading to an increase in the resistance of the hydrogel [26]. Therefore, the hydrogel is expected to be a competent sensing material.

The rheological measurement of CCNF-LM-PAA hydrogel shows that its storage modulus (G') is far larger than its loss modulus (Fig. S4), confirming the elastic solid-like nature of the hydrogel [46]. To further quantify their mechanical properties, hydrogels with different added Ga amounts and CCNF concentrations were prepared. According to Fig. 2j–k, the concentration of CCNFs and the added amount of Ga in the system have an obvious effect on the tensile strength and stretchability of the hydrogels. The tensile strength and toughness improve, but the elongation at break decreases with increasing CCNF concentration and Ga added amount (Fig. S5) because CCNFs form a rigid network to dissipate substantial amounts of energy during deformation [26], while Ga droplets react with H^+ to form Ga^{3+}, which induces ionic crosslinking among PAA molecules [49], both of which are conducive to increasing the resistance of hydrogels to deformation. Therefore, too much Ga^{3+} or excess CCNFs may make the hydrogel brittle. Combining cost savings with the discovery that the conductivity of the CCNF-LM-PAA hydrogels does not change remarkably with the amount of Ga (Fig. S6), we finally selected the hydrogel fabricated with a 0.4 wt% CCNF-stabilized LM emulsion containing 0.2 g of Ga, which has a tensile strength and toughness of 119 kPa and 1815 kJ m^{-3}, respectively, and sustains a large elongation at break of approximately 1674%. To further evaluate the fatigue resistance of the hydrogel prepared with a 0.4 wt%

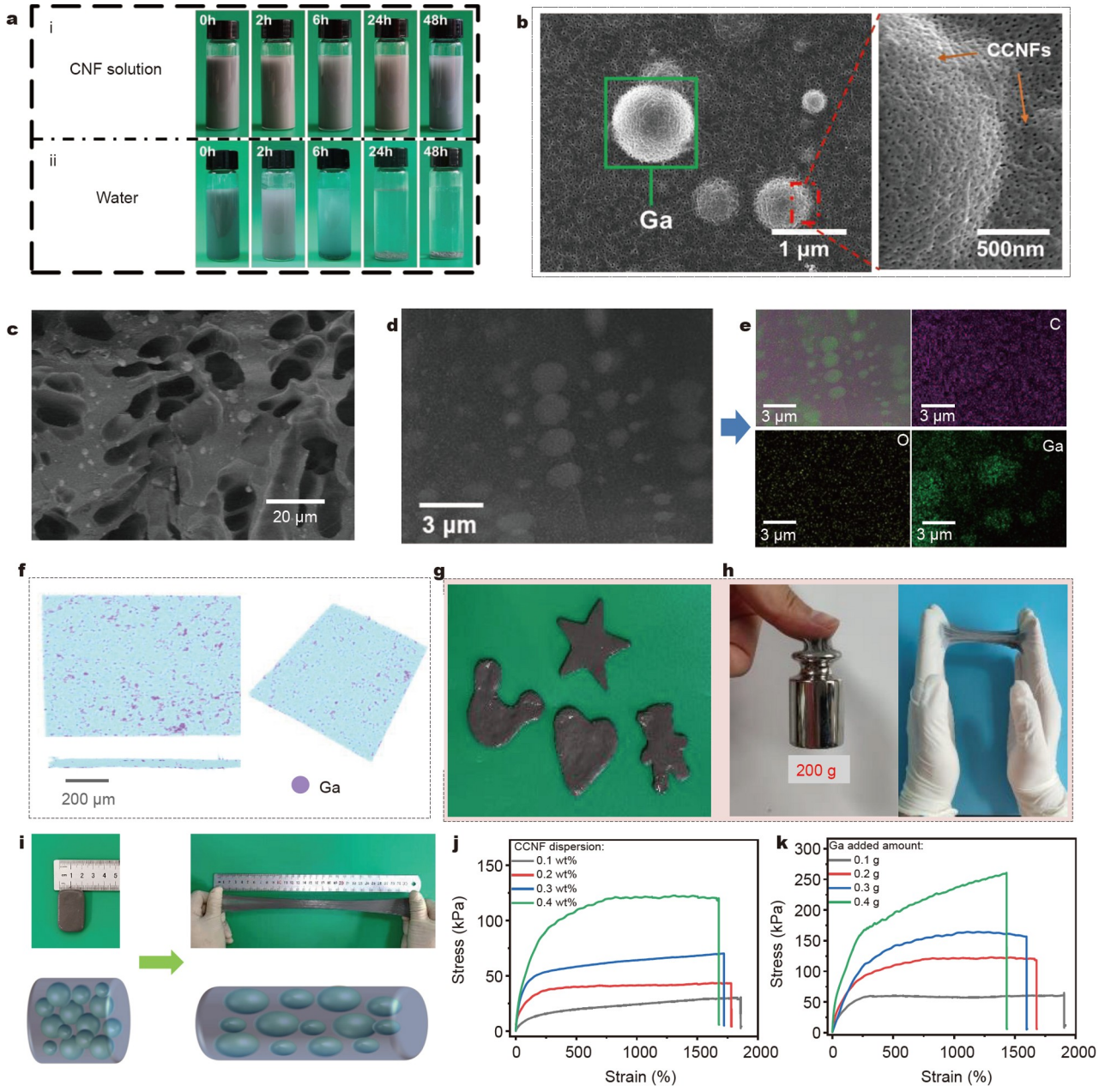

Figure 2 (a) Photographs of LM emulsions prepared by dispersing 0.2 g of Ga in (a-i) 0.2 wt% CCNFs, where the CCNF:Ga mass ratio is 0.14:2 and (a-ii) pure water as a function of the standing time. SEM images of (b) CCNF-stabilized LM droplets and (c) the cross-sectional CCNF-LM-PAA hydrogel with a CCNF:Ga:AA mass ratio of 0.14:2:27 after being freeze-dried. (d, e) SEM-EDS element map images of the CCNF-LM-PAA hydrogel showing the distribution of C, O, and Ga in the same region. (f) Micro-CT images of the CCNF-LM-PAA hydrogel. Photograph of (g) the CCNF-LM-PAA hydrogel with different shapes, (h) CCNF-LM-PAA hydrogel for lifting a 200-g weight by adhesiveness and adhering to rubber latex gloves, and (i) CCNF-LM-PAA hydrogel for showing stretchability. Stress-strain curves of CCNF-LM-PAA hydrogels fabricated by introducing CCNF-stabilized LM emulsions with (j) different concentrations of CCNFs, where Ga:AA is fixed at 2:27, and (k) different amounts of Ga, where the concentration of CCNFs is fixed at 0.4 wt%, and CCNF:AA is fixed at 0.28:27.

CCNF-stabilized LM emulsion containing 0.2 g of Ga, tensile loading-unloading cyclic tests were conducted at the strains of 100% and 150% for 10 cycles, respectively (Fig. S7). CCNF-LM-PAA hydrogel deformation is found to effectively dissipate some of the energy due to the fracture of the physically crosslinked network and LM droplet deformation during the loading process. The deformation at a strain of 150% induces larger energy dissipation than that at a strain of 100%. However, the energy dissipation after the first loading-unloading cycle becomes much smaller and can ensure hydrogel mechanical stability (Fig. S7). The recorded real-time tensile stress confirms that the CCNF-LM-PAA hydrogel has considerable mechanical stability to 150% strain, particularly after undergoing 15 cycles of stretching (Fig. S8). The excellent mechanical properties of the as-prepared CCNF-LM-PAA hydrogel lay a good foundation for its use as a wearable electronic skin.

Self-healing property

Self-healing is one of the most important properties of hydrogel-based strain sensors because it can minimize the effect of sudden

damage on the electrical and mechanical properties of sensing materials. To macroscopically show the self-healing property, as shown in Fig. 3a, two strips of CCNF-LM-PAA hydrogel were used to establish a connection between a yellow light-emitting diode (LED) indicator and a power source, enabling an LED indicator to be lit. When one strip of hydrogel was cut off, the LED indicator light was extinguished. Once the two cutoff parts were connected, the LED indicator could be relit, proving the self-healing ability of the CCNF-LM-PAA hydrogel [38]. The mechanical self-healing performance of the CCNF-LM-PAA hydrogel was further evaluated by conducting tensile tests to record its stress-strain curves before and after contact with the two cutoff parts for 20 min. As shown in Fig. 3b, the healed hydrogel recovered to approximately 82% of its original tensile stress within 20 min, confirming the excellent mechanical self-healing performance of the CCNF-LM-PAA hydrogel.

The electrical self-healing performance was investigated by recording the real-time current evolution of the CCNF-LM-PAA hydrogel during cutting-healing cycles under an external voltage of 1 V. The results are displayed in Fig. 3c, which shows that the healed hydrogel still sustains an almost constant current after being cut off eight times at the same position, suggesting a good self-healing performance of the hydrogel in electrical performance. Fig. 3d, e show a recorded cutting-healing cycle and the conductivity variation in the CCNF-LM-PAA hydrogel before being cut off and after being healed, respectively. According to Fig. 3d, e, the CCNF-LM-PAA hydrogel can restore its conductivity within 0.3 s after being cut off and connected together, and the restored conductivity is 1.541 S m^{-1}, which is almost identical to its initial value of 1.544 S m^{-1}, further verifying the quick and highly efficient self-healing performance of the CCNF-LM-PAA hydrogel in electrical conductivity. The good

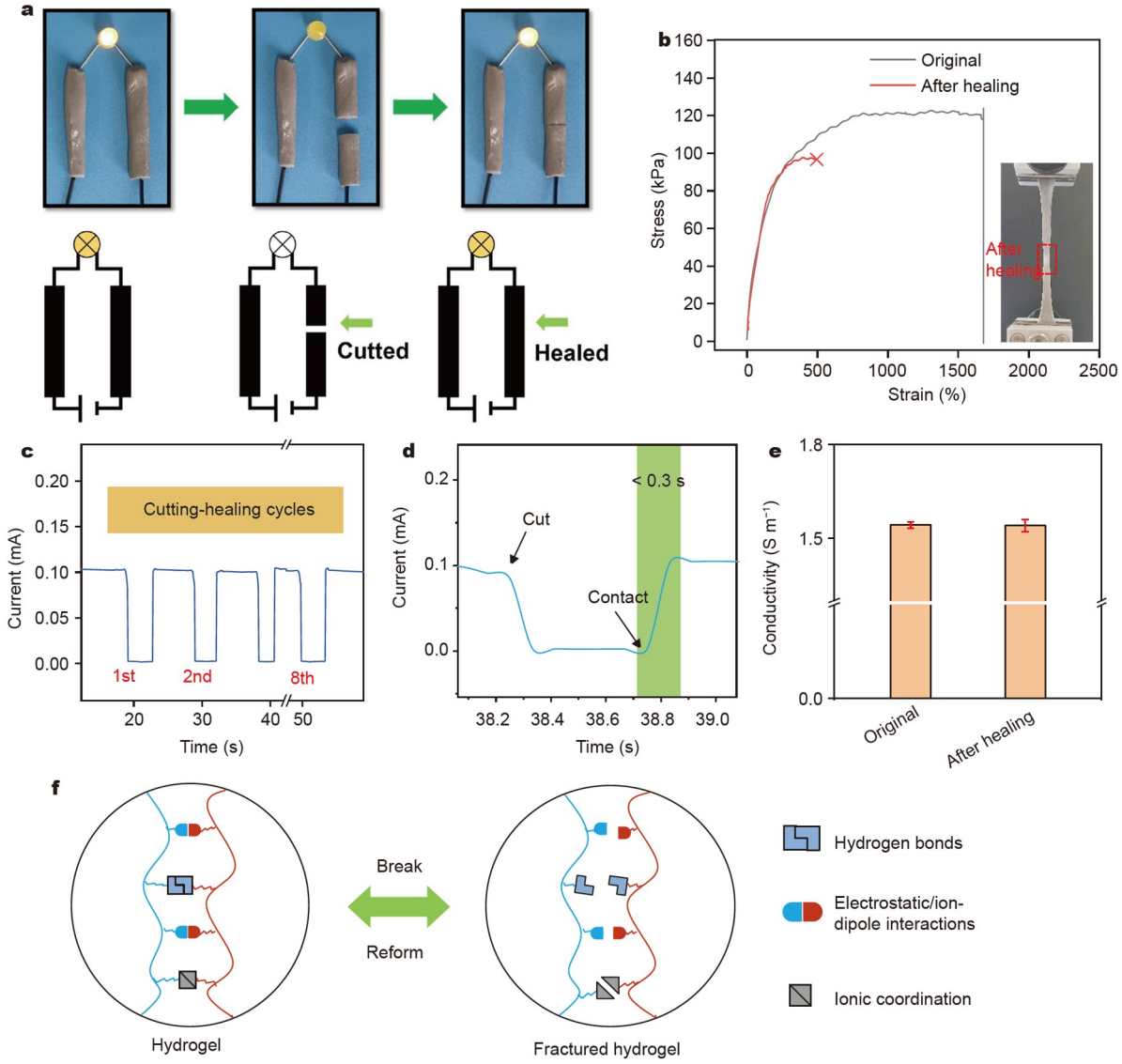

Figure 3 (a) Photographs and schematics showing the self-healing behavior of the CCNF-LM-PAA hydrogel as a conductor connected in a circuit with a yellow LED bulb. (b) Stress-strain curves of hydrogel before and after the contact of the two cutoff parts for 20 min (self-healing). (c) Current variations in the CCNF-LM-PAA hydrogel with successive cutting and contacting. (d) Time-dependent current and healing speed of the CCNF-LM-PAA hydrogel. (e) Conductivity of hydrogels before cutting and after self-healing. (f) Schematic of the self-healing process induced by hydrogen bonding and electrostatic interactions at the fracture interfaces.

self-healing performance of the CCNF-LM-PAA hydrogel in terms of mechanical and electrical properties originates from the reconstruction of the supramolecular network structure and electrically/ionically conductive pathways within the hydrogel network [38,48]. According to the reversibility of hydrogen bonding, ionic coordination, and electrostatic interactions among PAA, CCNFs, and Ga^{3+}, we proposed the self-healing mechanism of the CCNF-LM-PAA hydrogel shown in Fig. 3f. When the two halves of the cutoff hydrogel contact each other, self-healed supramolecular networks are reformed because of hydrogen bonding between the –COOH groups of PAA and the –OH groups of CCNFs, the ionic coordination between the $–COO^-$ groups of PAA and Ga^{3+}, and the electrostatic interaction between the $–COO^-$ groups of PAA and the $–N^+(CH_3)_3$ groups of CCNFs, recovering the mechanical strength of the CCNF-LM-PAA hydrogel by self-healing. Simultaneously, with the contact between the two halves of the cutoff hydrogel, the electrically conductive pathways composed of CCNF-stabilized LM droplets are established immediately, and ionic diffusion channels composed of crosslinked supramolecular networks are established with the crosslinking among PAA/CCNFs on the cutoff interfaces [36].

Sensing performance

Conductivity is a crucial property for conductive hydrogels to exert good sensing performance [26]. The CCNF-LM-PAA hydrogel shows high conductivity (1.544 S m^{-1}), which is derived from the well-dispersed Ga droplets, dissolved Ga^{3+}, $–N^+$, and $(CH_3)_3/Cl^-$ from CCNFs, $H^+/–COO^-$ from PAA, and even $NH_4^+/S_2O_8^{2-}$ from APS and does not change with the Ga content (Fig. S6). This phenomenon indicates that the Ga droplets may not form conductive networks within the hydrogel due to its low content [41], while the Ga^{3+} concentration is not proportional to the Ga content when the added amount of Ga exceeds 0.1 g. As illustrated in Fig. 4a, the CCNF-LM-PAA hydrogel can illuminate the LED as a conductor. The LED became darker with an increasing tensile strain of the CCNF-LM-PAA hydrogel and then recovered its original luminance immediately after unloading the strain, indicating a fast resistance response and high strain sensitivity of the CCNF-LM-PAA hydrogel.

Fig. 4b shows the relationship between the resistance and strain of the CCNF-LM-PAA hydrogel under different applied strains. Apparently, the resistance of the CCNF-LM-PAA hydrogel is only 3.83 kΩ without stretching. When a tensile strain of 25% is applied to the hydrogel, its resistance increases to 5.53 kΩ. Upon further increasing the applied tensile strain to 50%, 75%, and 100%, the resistance increases linearly to 7.14, 9.45, and 11.43 kΩ, respectively, further confirming the good conductivity and excellent response to the applied tensile strain of the CCNF-LM-PAA hydrogel. Furthermore, when the applied tensile strain is unloaded, the resistance recovers to its original value without hysteresis, indicating good hydrogel resilience.

The GF, which is defined as the slope of a plot of the relative resistance change *versus* strain, is generally used to evaluate the strain sensitivity and is calculated as the ratio of the relative resistance change ($(R - R_0)/R_0$) to the applied strain (ε), where R and R_0 represent the real-time and pristine resistance, respectively [54,55]. As depicted in Fig. 4c, the $(R - R_0)/R_0$ value of the CCNF-LM-PAA hydrogel increases with ε within the tested range of strain (0%–1000%). However, the plot of $(R - R_0)/R_0$ *versus* ε is not linear. This plot can be divided into three linear regions, as labeled in Fig. 4c. In the low ε region of 0%–250%, the calculated GF value is 2.7 for the CCNF-LM-PAA hydrogel-based strain sensor. In the middle ε region of 250%–675% and the high ε region of 675%–1000%, the calculated GF values are increased to 9.24 and 16.2, respectively. To our knowledge, this GF value is the highest one obtained from LM droplet-based conductive hydrogels up to now. The GF value of most LM droplet-based conductive hydrogel is less than 10 (Table S1). Even in the high strain range of 1500%–2000%, the highest GF value in the previous work is only 12.5 [48]. The high GF, which originates from the high conductivity of the hydrogel and its multiple conductive modes, indicates the high sensitivity of the CCNF-LM-PAA hydrogel-based strain sensor.

Fig. 4d–f show the typical real-time $(R - R_0)/R_0$ of the CCNF-LM-PAA hydrogel-based strain sensor with cyclic loading and unloading of ε in the low to intermediate ε regions. As shown in the figures, all the $(R - R_0)/R_0$ *versus* time curves of the CCNF-LM-PAA hydrogel-based strain sensor are regular and repeatable pulses with the same frequency as the loading and unloading frequency of ε. The maximum value of the pulses is proportional to the applied ε, further confirming the good relationship between the $(R - R_0)/R_0$ output and the applied ε. The repeatability of the outputs is due to the excellent resilience of the CCNF-LM-PAA hydrogel. Meanwhile, even for the cyclic loading and unloading at a small strain of 1%, the CCNF-LM-PAA hydrogel-based strain sensor still outputs regular and repeatable pulses with a maximum $(R - R_0)/R_0$ value higher than 1.5% (Fig. 4e), demonstrating that the sensor detection limit for tensile strain is lower than 1%. Furthermore, the real-time $(R - R_0)/R_0$ values of the CCNF-LM-PAA hydrogel-based strain sensor at an applied ε of 50% under different loading and unloading frequencies were recorded in Fig. 4g. As shown in Fig. 4g, the recorded $(R - R_0)/R_0$ *versus* time curves have the same maximum value under different frequencies from 0.5 to 2 Hz, demonstrating the excellent output performance of the sensor to strain which is independent of the loading and unloading frequency.

Response/recovery time is an important parameter for a strain sensor. To obtain the response/recovery time of the CCMF-LM-PAA hydrogel-based strain sensor, a tensile strain of approximately 1.2% was applied by manual stretching, and this stretching state could be maintained for some time. The result is shown in Fig. 4h, which indicates that the CCNF-LM-PAA hydrogel-based strain sensor has a very short response time of 107 ms and an even shorter recovery time of 91 ms. The quick response of the CCNF-LM-PAA hydrogel-based strain sensor is due to the high resilience of the hydrogel. The sensing stability is also crucial for a strain sensor, particularly when used as electronic skin. To evaluate the sensing stability of the CCNF-LM-PAA hydrogel-based strain sensor, 50% ε was repeatedly loaded and unloaded on the strain sensors for 300 cycles. Fig. 4i shows the real-time $(R - R_0)/R_0$ output of the CCNF-LM-PAA hydrogel-based strain sensor under a cyclic tensile strain of 50%. As shown in Fig. 4i, the $(R - R_0)/R_0$ *versus* time curves comprise a series of pulses with similar shapes and amplitudes before the loading and unloading of the applied ε reaches 250 cycles, indicating that the CCNF-LM-PAA hydrogel-based strain sensor has excellent sensing stability at low tensile strain. When a high cyclic tensile strain of 150% is applied to the CCNF-LM-PAA hydrogel-based strain sensor at a reduced frequency, the sensing

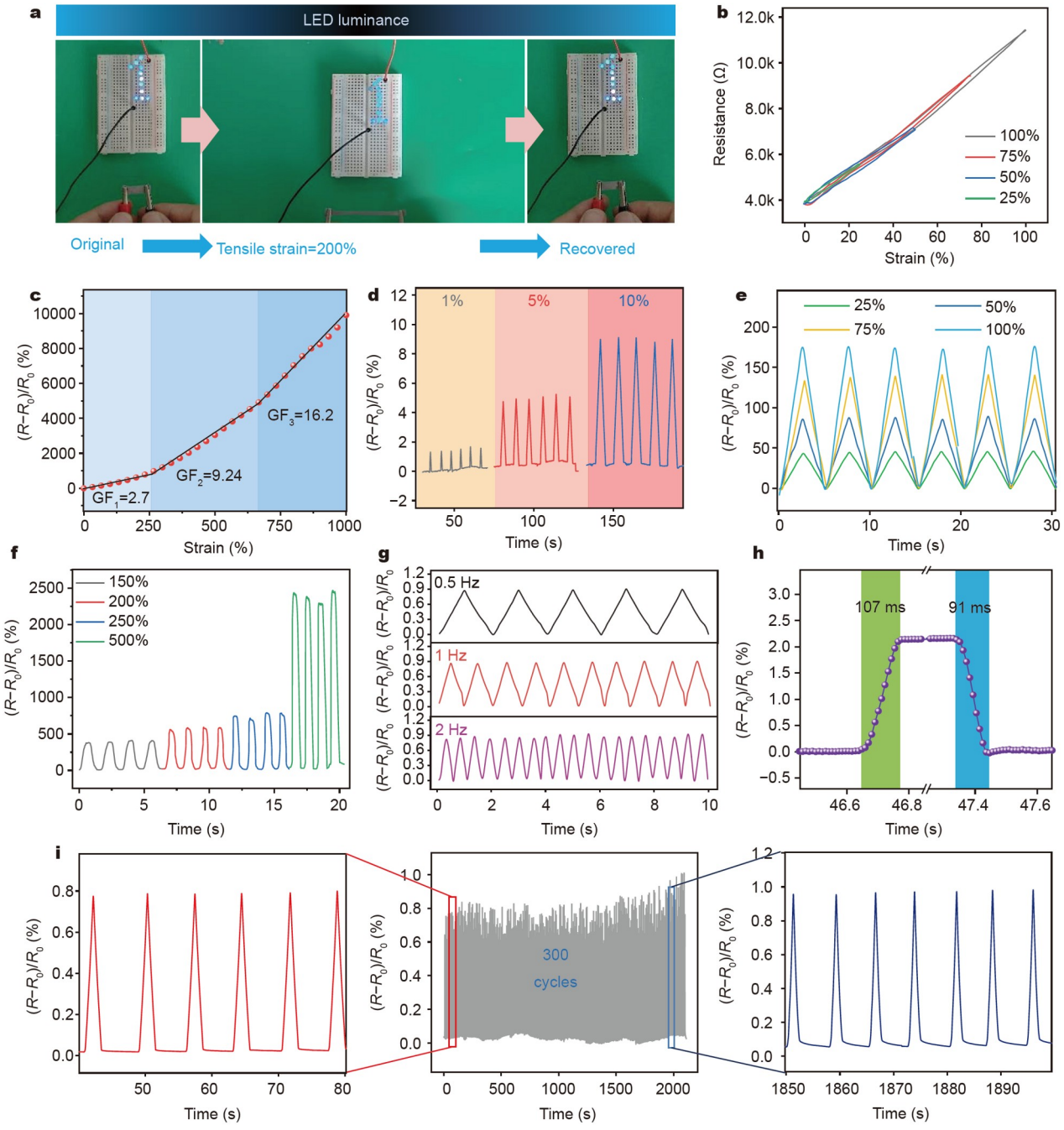

Figure 4 (a) Luminance variations of an LED with a stretching-releasing cycle of the CCNF-LM-PAA hydrogel, which is used to connect the power supply. (b) Resistance of the hydrogel to different strains during tensile loading-unloading cycles. (c) Relative resistance change of the CCNF-LM-PAA hydrogel as a function of tensile strain. (d–f) Real-time relative resistance changes of the CCNF-LM-PAA hydrogel under various cyclic tensile strains. (g) Relative resistance changes of the CCNF-LM-PAA hydrogel under various cyclic tensile frequencies and (h) the corresponding response and recovery times under 1 Hz. (i) Relative resistance changes under a cyclic tensile strain of 50% for more than 300 cycles and an enlarged view of the marked region showing the excellent stability and repeatability of the CCNF-LM-PAA hydrogel-based sensor.

stability is even improved within 100 cycles (Fig. S9).

Application in monitoring human activity

Its good moldability, adhesiveness, self-healing capacity, and excellent sensing performance qualify the CCNF-LM-PAA hydrogel as a potential sensing material for wearable devices to monitor various human activities. To demonstrate its monitoring capabilities as a strain-sensing material, the hydrogel-based strain sensor is directly attached to the finger of a volunteer for recording the real-time value of $(R - R_0)/R_0$ induced by finger bending, and the results are shown in Fig. 5a, b. As shown in Fig. 5a, when the finger bends stepwise from 0° to 90° and straightens from 90° to 0°, the CCNF-LM-PAA hydrogel-based strain sensor produces a stepwise increase and a stepwise decrease in $(R - R_0)/R_0$, respectively, due to the stretching and recovery of the hydrogel, while $(R - R_0)/R_0$ has the same value at

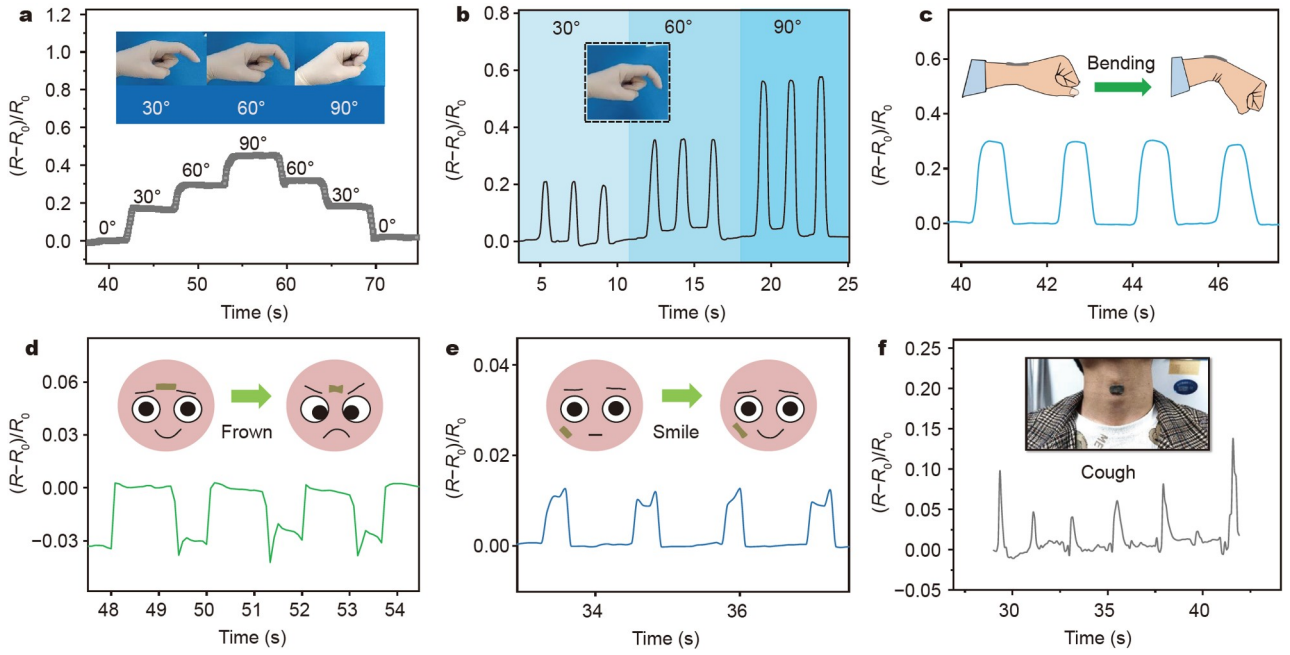

Figure 5 Relative resistance change of the CCNF-LM-PAA hydrogel-based strain sensor in response to (a, b) finger bending, (c) wrist bending, (d) frowning, and (e) smiling. The insets show the motions and experimental setup. Each motion was repeated four times. (f) Relative resistance change of the CCNF-LM-PAA hydrogel-based strain sensor in response to coughing. The inset shows that the sensor can be directly attached to the neck by self-adhesiveness.

the same bending angle during the bending and straightening process. Meanwhile, as shown in Fig. 5b, quickly and repeatedly bending the finger at different angles makes the strain sensor output real-time repeatable pulses with the maximum value proportional to the bending angle.

Similarly, when the CCNF-LM-PAA hydrogel-based strain sensor is self-attached to the wrist of the volunteer and bends with the wrist periodically, as shown in Fig. 5c, it outputs real-time pulses with the same morphology and the corresponding maximum value. Therefore, the CCNF-LM-PAA hydrogel-based strain sensor shows a repeatable and proportioned response to joint bending owing to its good sensing performance and self-adhesiveness that allows it to conformably stick to the skin.

In addition to large human motion, such as finger and wrist bending, the hydrogel-based strain sensor was also used to detect subtle changes in human facial expressions. Fig. 5d shows the real-time response of the CCNF-LM-PAA hydrogel-based strain sensor to frowning when it is self-attached to the forehead of the volunteer. As shown in Fig. 5d, regular and strong real-time output with $(R - R_0)/R_0$ less than 0 is produced because of the compression of the hydrogel produced by frowning. Meanwhile, the slight differences in each frown lead to a slight difference in the shape of each $(R - R_0)/R_0$ *versus* time curve, indicating the sensitive response of the strain sensor to the subtle motion of the human body.

When the hydrogel-based strain sensor is attached to the cheek of the volunteer, as shown in Fig. 5e, the smile of the volunteer causes stretching, thus increasing the $(R - R_0)/R_0$ value of the hydrogel. Unsurprisingly, the shape of each $(R - R_0)/R_0$ *versus* time curve slightly changes with the slight difference of each smile. Therefore, the CCNF-LM-PAA hydrogel-based strain sensor can detect the changes in facial expression. To further monitor the tiny motion induced by throat vibration, the CCNF-LM-PAA hydrogel-based strain sensor was self-attached to the throat of the volunteer to monitor the real-time variation in $(R - R_0)/R_0$ with coughing, and the results are shown in Fig. 5f. Apparently, the throat vibration induced by coughing makes the hydrogel-based strain sensor output sharp peaks with maximum values larger than that induced by facial expressions and proportional to the cough strength, indicating that the hydrogel-based strain sensor can accurately detect tiny throat vibrations.

CONCLUSIONS

In summary, this work demonstrated a strategy for stabilizing LM emulsions by encapsulating LM droplets with CCNFs, which formed mechanical barriers to prevent the LM droplets from coalescing and undergoing sedimentation. The encapsulated LM droplets had a diameter of 0.25–1.0 μm and were incorporated into the hydrogel by being added into AA, which was *in situ* polymerized and crosslinked to form the polymeric networks together with CCNFs. As a conductive filler, the reservoirs of an ionic crosslinking agent (Ga^{3+}) and a hard network-forming component, the CCNF-stabilized LM emulsion constituted a CCNF-LM-PAA hydrogel together with *in situ* synthesized PAA through reversible hydrogen bonds, ionic coordination, and electrostatic interactions. The multiple functions of the CCNF-stabilized LM emulsion allowed the CCNF-LM-PAA hydrogel to show good conductivity (1.54 S m^{-1}), remarkable mechanical properties, self-adhesiveness, and quick self-healing capability. As a strain-sensing material, the CCNF-LM-PAA hydrogel exhibited a very high sensing sensitivity (GF = 16.2), a low strain detection limit (less than 1%), a short response/recovery time (107/91 ms), and good repeatability and durability. The excellent sensing performance, self-adhesiveness and self-healing capacity also make the CCNF-LM-PAA hydrogel-based strain sensor competent for monitoring various human activities, including large motions (such as bending fingers and wrists), subtle

motions (such as frowning and smiling), and tiny motions (such as throat vibrations induced by coughing). Therefore, using CCNFs to stabilize LM emulsions enabled the LM-based hydrogel to be a potential sensing material for self-attached wearable devices.

Received 26 August 2022; accepted 15 November 2022; published online 18 January 2023

1 Chen B, Dong J, Ruelas M, *et al.* Artificial intelligence-assisted high-throughput screening of printing conditions of hydrogel architectures for accelerated diabetic wound healing. Adv Funct Mater, 2022, 32: 2201843
2 Whitesides GM. Soft robotics. Angew Chem Int Ed, 2018, 57: 4258–4273
3 Wang H, Totaro M, Beccai L. Toward perceptive soft robots: Progress and challenges. Adv Sci, 2018, 5: 1800541
4 He S, Cheng Q, Liu Y, *et al.* Intrinsically anti-freezing and anti-dehydration hydrogel for multifunctional wearable sensors. Sci China Mater, 2022, 65: 1980–1986
5 Peng X, Wang W, Yang W, *et al.* Stretchable, compressible, and conductive hydrogel for sensitive wearable soft sensors. J Colloid Interface Sci, 2022, 618: 111–120
6 Kim Y, Chortos A, Xu W, *et al.* A bioinspired flexible organic artificial afferent nerve. Science, 2018, 360: 998–1003
7 Wang L, Chen D, Jiang K, *et al.* New insights and perspectives into biological materials for flexible electronics. Chem Soc Rev, 2017, 46: 6764–6815
8 Peng H, Xin Y, Xu J, *et al.* Ultra-stretchable hydrogels with reactive liquid metals as asymmetric force-sensors. Mater Horiz, 2019, 6: 618–625
9 Wang Y, Liu Y, Hu N, *et al.* Highly stretchable and self-healable ionogels with multiple sensitivity towards compression, strain and moisture for skin-inspired ionic sensors. Sci China Mater, 2022, 65: 2252–2261
10 Bai J, Wang R, Ju M, *et al.* Facile preparation and high performance of wearable strain sensors based on ionically cross-linked composite hydrogels. Sci China Mater, 2021, 64: 942–952
11 Yu R, Xia T, Wu B, *et al.* Highly sensitive flexible piezoresistive sensor with 3D conductive network. ACS Appl Mater Interfaces, 2020, 12: 35291–35299
12 Wang YF, Sekine T, Takeda Y, *et al.* Fully printed PEDOT:PSS-based temperature sensor with high humidity stability for wireless healthcare monitoring. Sci Rep, 2020, 10: 2467
13 Shin J, Jeong B, Kim J, *et al.* Sensitive wearable temperature sensor with seamless monolithic integration. Adv Mater, 2020, 32: 1905527
14 Wang Y, Zhang L, Zhang Z, *et al.* High-sensitivity wearable and flexible humidity sensor based on graphene oxide/non-woven fabric for respiration monitoring. Langmuir, 2020, 36: 9443–9448
15 Wang Y, Zhang L, Zhou J, *et al.* Flexible and transparent cellulose-based ionic film as a humidity sensor. ACS Appl Mater Interfaces, 2020, 12: 7631–7638
16 Khan A, Kisannagar RR, Gouda C, *et al.* Highly stretchable supramolecular conductive self-healable gels for injectable adhesive and flexible sensor applications. J Mater Chem A, 2020, 8: 19954–19964
17 Cao J, He G, Ning X, *et al.* Hydroxypropyl chitosan-based dual self-healing hydrogel for adsorption of chromium ions. Int J Biol Macromolecules, 2021, 174: 89–100
18 Deng Z, Guo Y, Zhao X, *et al.* Multifunctional stimuli-responsive hydrogels with self-healing, high conductivity, and rapid recovery through host-guest interactions. Chem Mater, 2018, 30: 1729–1742
19 Deng Z, Wang H, Ma PX, *et al.* Self-healing conductive hydrogels: Preparation, properties and applications. Nanoscale, 2020, 12: 1224–1246
20 Matsuda T, Kawakami R, Namba R, *et al.* Mechanoresponsive self-growing hydrogels inspired by muscle training. Science, 2019, 363: 504–508
21 Liu X, Liu J, Lin S, *et al.* Hydrogel machines. Mater Today, 2020, 36: 102–124
22 Bai J, Wang R, Wang X, *et al.* Biomineral calcium-ion-mediated conductive hydrogels with high stretchability and self-adhesiveness for sensitive iontronic sensors. Cell Rep Phys Sci, 2021, 2: 100623
23 Gao Y, Gu S, Jia F, *et al.* A skin-matchable, recyclable and biofriendly strain sensor based on a hydrolyzed keratin-containing hydrogel. J Mater Chem A, 2020, 8: 24175–24183
24 Yang F, Zhao J, Koshut WJ, *et al.* A synthetic hydrogel composite with the mechanical behavior and durability of cartilage. Adv Funct Mater, 2020, 30: 2003451
25 Song J, Yuan C, Jiao T, *et al.* Multifunctional antimicrobial biometallohydrogels based on amino acid coordinated self-assembly. Small, 2020, 16: 1907309
26 Li G, Li C, Li G, *et al.* Development of conductive hydrogels for fabricating flexible strain sensors. Small, 2022, 18: 2101518
27 Li Q, Liu C, Wen J, *et al.* The design, mechanism and biomedical application of self-healing hydrogels. Chin Chem Lett, 2017, 28: 1857–1874
28 Wang X, Wang X, Yin J, *et al.* Mechanically robust, degradable and conductive MXene-composited gelatin organohydrogel with environmental stability and self-adhesiveness for multifunctional sensor. Compos Part B-Eng, 2022, 241: 110052
29 Zhao W, Han Z, Ma L, *et al.* Highly hemo-compatible, mechanically strong, and conductive dual cross-linked polymer hydrogels. J Mater Chem B, 2016, 4: 8016–8024
30 You L, Shi X, Cheng J, *et al.* Flexible porous gelatin/polypyrrole/reduction graphene oxide organohydrogel for wearable electronics. J Colloid Interface Sci, 2022, 625: 197–209
31 Shi Y, Ma C, Peng L, *et al.* Conductive "smart" hybrid hydrogels with PNIPAM and nanostructured conductive polymers. Adv Funct Mater, 2015, 25: 1219–1225
32 Deng Z, Yu R, Guo B. Stimuli-responsive conductive hydrogels: Design, properties, and applications. Mater Chem Front, 2021, 5: 2092–2123
33 Wang M, Feng X, Wang X, *et al.* Facile gelation of a fully polymeric conductive hydrogel activated by liquid metal nanoparticles. J Mater Chem A, 2021, 9: 24539–24547
34 Guo X, Ding Y, Xue L, *et al.* A self-healing room-temperature liquid-metal anode for alkali-ion batteries. Adv Funct Mater, 2018, 28: 1804649
35 Kazem N, Bartlett MD, Majidi C. Extreme toughening of soft materials with liquid metal. Adv Mater, 2018, 30: 1706594
36 Wang H, Yao Y, He Z, *et al.* A highly stretchable liquid metal polymer as reversible transitional insulator and conductor. Adv Mater, 2019, 31: 1901337
37 Yuk H, Lu B, Zhao X. Hydrogel bioelectronics. Chem Soc Rev, 2019, 48: 1642–1667
38 Liao M, Liao H, Ye J, *et al.* Polyvinyl alcohol-stabilized liquid metal hydrogel for wearable transient epidermal sensors. ACS Appl Mater Interfaces, 2019, 11: 47358–47364
39 Zhou Z, Qian C, Yuan W. Self-healing, anti-freezing, adhesive and remoldable hydrogel sensor with ion-liquid metal dual conductivity for biomimetic skin. Compos Sci Tech, 2021, 203: 108608
40 Choi YY, Ho DH, Cho JH. Self-healable hydrogel-liquid metal composite platform enabled by a 3D printed stamp for a multimodular sensor system. ACS Appl Mater Interfaces, 2020, 12: 9824–9832
41 Xu J, Wang Z, You J, *et al.* Polymerization of moldable self-healing hydrogel with liquid metal nanodroplets for flexible strain-sensing devices. Chem Eng J, 2020, 392: 123788
42 Yang Z, Yang D, Zhao X, *et al.* From liquid metal to stretchable electronics: Overcoming the surface tension. Sci China Mater, 2022, 65: 2072–2088
43 Wang C, Li J, Fang Z, *et al.* Temperature-stress bimodal sensing conductive hydrogel-liquid metal by facile synthesis for smart wearable sensor. Macromol Rapid Commun, 2022, 43: 2100543
44 Tang R, Meng Q, Wang Z, *et al.* Multifunctional ternary hybrid hydrogel sensor prepared *via* the synergistic stabilization effect. ACS Appl Mater Interfaces, 2021, 13: 57725–57734
45 Hao X, Li N, Wang H, *et al.* Dialdehyde xylan-based sustainable, stable, and catalytic liquid metal nano-inks. Green Chem, 2021, 23: 7796–7804

46 Hu Y, Zhuo H, Zhang Y, *et al.* Graphene oxide encapsulating liquid metal to toughen hydrogel. Adv Funct Mater, 2021, 31: 2106761
47 Zhang Z, Tang L, Chen C, *et al.* Liquid metal-created macroporous composite hydrogels with self-healing ability and multiple sensations as artificial flexible sensors. J Mater Chem A, 2021, 9: 875–883
48 Ye Y, Jiang F. Highly stretchable, durable, and transient conductive hydrogel for multi-functional sensor and signal transmission applications. Nano Energy, 2022, 99: 107374
49 Wang XP, Guo JR, Hu L. Preparation and application of gallium-based conductive materials in the very recent years. Sci China Technol Sci, 2021, 64: 681–695
50 Wang J, Dai T, Wu H, *et al.* Tannic acid-Fe^{3+} activated rapid polymerization of ionic conductive hydrogels with high mechanical properties, self-healing, and self-adhesion for flexible wearable sensors. Compos Sci Tech, 2022, 221: 109345
51 Zhang X, Chen J, He J, *et al.* Mussel-inspired adhesive and conductive hydrogel with tunable mechanical properties for wearable strain sensors. J Colloid Interface Sci, 2021, 585: 420–432
52 Zhang X, Wang D, Liu H, *et al.* A nucleobase-inspired super adhesive hydrogel with desirable mechanical, tough and fatigue resistant properties based on cytosine and ε-caprolactone. Eur Polym J, 2020, 133: 109741
53 Chen J, He J, Yang Y, *et al.* Antibacterial adhesive self-healing hydrogels to promote diabetic wound healing. Acta Biomater, 2022, 146: 119–130
54 Cai G, Wang J, Qian K, *et al.* Extremely stretchable strain sensors based on conductive self-healing dynamic cross-links hydrogels for human-motion detection. Adv Sci, 2017, 4: 1600190
55 Shao C, Wang M, Meng L, *et al.* Mussel-inspired cellulose nanocomposite tough hydrogels with synergistic self-healing, adhesive, and strain-sensitive properties. Chem Mater, 2018, 30: 3110–3121

Acknowledgements This work was supported by the National Natural Science Foundation of China (52172147 and 22006082), the Natural Science Foundation of Shandong Province (ZR2021MC034, ZR2021MB035, and ZR2020MB128), and Shandong Province Key Research and Development Program (2021ZDSYS18).

Author contributions Wu S and Wang B carried out the experiments and collected the data. Wu S and Liu W conceived the idea, designed the experiments, analyzed the data and wrote the paper. Liu W supervised the project. Chen D and Ge S provided the methodology. Liu X, Wang H, Song Z, Yu D and Li G analyzed the data and prepared the figures. All authors contributed to the general discussion.

Conflict of interest The authors declare that they have no conflict of interest.

Supplementary information Supporting data are available in the online version of this paper.

Shihao Wu received his Master's degree from the State Key Laboratory of Biobased Material and Green Papermaking, Qilu University of Technology, China. He received his Bachelor's degree in bioengineering from Henan University of Science and Technology, China, in 2019. His current research interests focus on cellulose-based flexible electronic devices.

Bingyan Wang is currently a graduate student at the State Key Laboratory of Biobased Material and Green Papermaking, Qilu University of Technology, China. She received her Bachelor's degree in food science and engineering from Shandong University of Technology, China, in 2020. Her current research interests focus on biomaterial-based flexible electronic devices.

Wenxia Liu is currently a professor at the State Key Laboratory of Biobased Materials and Green Papermaking, Qilu University of Technology, China. She received her Bachelor's and Master's degrees in pulp and paper engineering from Shaanxi University of Science and Technology, China, in 1985 and 1988, respectively. She joined the Faculty of Pulp and Paper Engineering at Qilu University of Technology in 1988. In 2000, she received her doctoral degree in pulp and paper engineering from Tianjin University of Science and Technology, China. Her research interests focus on paper wet-end chemistry, nanomaterials, and paper and biomass-based flexible materials.

阳离子纤维素纳米纤维分散液态金属制备高灵敏度和自修复导电水凝胶用于应变传感器

武世豪[1†], 王炳艳[1†], 陈铎[2], 刘小娜[1], 王慧丽[1], 宋兆萍[1], 于得海[1], 李国栋[1], 葛少华[3], 刘温霞[1*]

摘要 作为一种多功能软填料，液态金属(LM)乳液为制备基于导电水凝胶的多功能应变传感器带来了新机遇. 然而, 界面张力和密度巨大的LM难以以稳定乳液的形式存在. 本文中，我们展示了一种利用阳离子纤维素纳米纤维(CCNFs)包覆LM液滴来稳定LM乳液的策略. 通过将CCNF稳定的LM乳液与丙烯酸(AA)混合并引发其原位聚合，以及在聚丙烯酸(PAA)、LM液滴和CCNF之间形成可逆的氢键、离子配位键和静电交联，制备了一种导电水凝胶CCNF-LM-PAA. 得益于PAA与CCNF之间形成的可逆氢键、离子配位键和静电结合作用，CCNF-LM-PAA水凝胶具有良好的导电性(1.54 S m^{-1})、较高的拉伸强度和断裂伸长率、粘附性和快速自愈合能力. CCNF-LM-PAA水凝胶作为应变传感材料，具有超高应变灵敏度(应变系数高达16.2)、低应变检测极限(<1%)、短响应/恢复时间(107/91 ms)和良好的耐用性(300次循环). 这些性能使得基于CCNF-LM-PAA水凝胶的应变传感器能够作为可穿戴电子器件用于监测各种人体活动. 因此, 利用CCNF稳定LM乳液引入静电结合作用，为提高基于LM乳液水凝胶的可穿戴电子器件的应变传感性能提供了一种实用的方法.